TOC: Localizing Wireless Rechargeable Sensors with Time of Charge

YUANCHAO SHU and PENG CHENG, Zhejiang University
YU GU, Singapore University of Technology and Design
JIMING CHEN, Zhejiang University
TIAN HE, University of Minnesota

The wireless rechargeable sensor network is a promising platform for long-term applications such as inventory management, supply chain monitoring, and so on. For these applications, sensor localization is one of the most fundamental challenges. Different from a traditional sensor node, a wireless rechargeable sensor has to be charged above a voltage level by the wireless charger in order to support its sensing, computation, and communication operations. In this work, we consider the scenario where a mobile charger stops at different positions to charge sensors and propose a novel localization design that utilizes the unique *Time of Charge* (TOC) sequences among wireless rechargeable sensors. Specifically, we introduce two efficient region dividing methods, *Internode Division* and *Interarea Division*, to exploit TOC differences from both temporal and spatial dimensions to localize individual sensor nodes. To further optimize the system performance, we introduce both an optimal charger stop planning algorithm for the single-sensor case and a suboptimal charger stop planning algorithm for the generic multisensor scenario with a provable performance bound. We have extensively evaluated our design by both testbed experiments and large-scale simulations. The experiment and simulation results show that by as less as five stops, our design can achieve sub-meter accuracy and the performance is robust under various system conditions.

Categories and Subject Descriptors: C.2.m [**Computer-Communication Networks**]: Miscellaneous

General Terms: Design, Algorithms, Performance

Additional Key Words and Phrases: Wireless rechargeable sensor networks, localization

ACM Reference Format:
Yuanchao Shu, Peng Cheng, Yu Gu, Jiming Chen, and Tian He. 2015. TOC: Localizing wireless rechargeable sensors with time of charge. ACM Trans. Sensor Netw. 11, 3, Article 44 (February 2015), 22 pages.
DOI: http://dx.doi.org/10.1145/2700257

1. INTRODUCTION

The wireless rechargeable sensor network (WRSN) is an emerging technology that integrates sensing, communication, and computation capabilities. Different from the traditional sensor nodes powered by batteries, wireless rechargeable sensor nodes gather their energy from the transmission of energy sources such as RFID readers. Given its small form factors and universal sensing capabilities, it is expected that the wireless rechargeable sensor will be a promising platform for different applications such as

Part of this work was published in the Proceedings of the IEEE INFOCOM 2014.
Research was supported in part by NSFC under grants 61222305, 61228302, 111 Program under grant B07031, NCET-11-0445, National Program for Special Support of Top-Notch Young Professionals.
Authors' addresses: Y. Shu, P. Cheng, and J. Chen (corresponding author), Department of Control Science and Engineering, Zhejiang University; emails: ycshu@zju.edu.cn and {pcheng, jmchen}@iipc.zju.edu.cn; Y. Gu, IBM Research, Austin; email: yugu@us.ibm.com; T. He, Department of Computer Science and Engineering, University of Minnesota; email: tianhe@cs.umn.edu.

DOI: http://dx.doi.org/10.1145/2700257

warehouse inventory management [Bijwaard et al. 2011; Liu et al. 2006], supply chain and environmental monitoring [Poon et al. 2009], authentication [Shu et al. 2014b; Yang et al. 2010], and so on.

For many such applications, the locations of sensor nodes are required for them to function properly. For example, for warehouse inventory management or environmental monitoring, it is usually necessary to identify the location where sensor readings originated from, which further benefits the robot-assisted search and delivery. Localization and tracking of RFID-based nodes can help supermarkets better understand consumers' shopping habits [Yang et al. 2014] and provide significant benefits in the hospital care environment and rescue services. For example, it facilitates medical equipment tracking under emergency situations and enables the detection of firefighters in buildings on fire or victims under the wall. In addition, some geographic routing protocols and network management optimization [Karp and Kung 2000; Kim et al. 2005] can only be implemented with given locations of sensor nodes.

For traditional wireless sensor networks, there are numerous localization methods that utilize the arrival sequences of a specific signal source to localize sensors, for example, time of arrival (TOA), angle of arrival (AOA), time difference of arrival (TDOA), and so forth [He et al. 2003]. Different from traditional approaches, in this work we exploit the *unique* wireless charging properties of the wireless rechargeable sensor nodes and propose the concept of Time of Charge (TOC), the time for a sensor node to be charged above its working threshold to localize individual nodes in a WRSN.

In this article, we consider the scenario in which a mobile charger moves and stops at different locations to wirelessly charge nodes and obtain the TOC for nodes in its surrounding area. It typically refers to a warehouse or supermarket where patrol readers monitor the status of goods (e.g., temperature, moisture) reported by attached wireless rechargeable sensors. The novel idea of TOC is to estimate each sensor's location by utilizing TOC sequences from both the temporal and spatial domains. Furthermore, TOC also optimizes the charger stop positions based on the estimated sensor locations.

TOC offers several unique benefits over traditional methods. First, compared with traditional methods such as TOA, AOA, and TDOA, which rely on the *instantaneous* readings from a specific signal source, TOC is an *accumulative* reading, which is more robust and resilient to transient signal fluctuations. Second, compared with the range-based approach, TOC does not require additional costly hardware. It works with existing components of WRSN nodes such as differential comparators and real-time clocks (RTCs). Third, compared with many range-free approaches, TOC only leverages the mobile charger in WRSN and does not require any anchor node, which reduces the infrastructure cost. Fourth, TOC is only based on the fact that charging time monotonically increases when the distance increases and does not have any assumption on the specific charging model, making it compatible with different types of wireless rechargeable sensor networks [Sample et al. 2008] and designs in mobile sensor networks [Abdulla et al. 2012; Zhuang et al. 2011; He et al. 2012; Cao et al. 2008].

This article offers the following intellectual contributions:

—To the best of our knowledge, this is the first work designed for localizing wireless rechargeable sensor nodes based on the Time of Charge sequences. We identify the fundamental relationship between the charging time and the distance between wireless rechargeable sensor nodes and the charger, based on which we propose the Time of Charge sequence-based localization design (TOC).
—We introduce two novel area division methods for localizing sensors, that is, *Internode Division* and *Interarea Division*, which exploit TOC differences among sensors from the time and spatial domains, respectively.

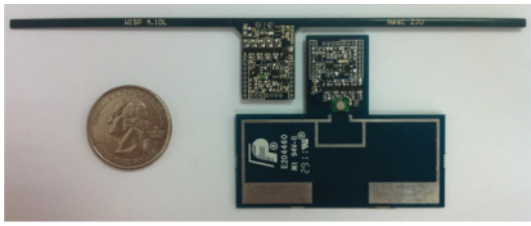

Fig. 1. Two types of WISP nodes.

—We propose an optimal charger stop solution for locating a single-sensor node. For the more general multisensor scenario, we introduce a suboptimal solution with a provable approximation ratio.
—We have implemented our TOC design on a physical testbed. The experiment results show that by as little as five stops, we can achieve submeter localization accuracy for a wireless rechargeable sensor network.

The remainder of this article is organized as follows. We introduce some preliminary knowledge of charging pattern in Section 2. In Section 3, we define the localization problem and propose the basic design of TOC. In Section 4, we propose the extended TOC algorithms. In Section 5, we discuss the impact of occasional charging time flips and provide corresponding solutions. We extensively evaluate TOC through testbed experiments and large-scale simulations in Section 6. Most related works are discussed in Section 7. Finally, we conclude in Section 8.

2. PRELIMINARY

One of the most common wireless rechargeable sensor nodes is the Wireless Identification Sensing Platform (WISP) developed by Intel Research [Sample et al. 2008]. WISP is a fully passive ultra-high-frequency (UHF) RFID tag that integrates a processor and several low-power sensors such as accelerometers and temperature sensors. Figure 1 shows two WISP nodes fabricated at our lab with different shapes of antenna. Through its antenna, a WISP node accumulates energy from signals of nearby standard UHF RFID readers (the charger) and stores the harvested energy in its capacitor for communication and powering other components of the node.

For the charging process, the exact charging model is usually difficult to obtain due to factors such as polarization and antenna impedance. However, one of our major observations is that the charging power is typically negatively correlated to the relative distance between the wireless rechargeable node and the energy source, for example, the charger. Many mathematical analyses and experimental results also prove there exists a negative correlation between the charging power and distance [He et al. 2013]. To verify this observation, we conducted a series of experiments using our fabricated WISP with a capacitor of $100\mu F$ and a charger with transmission power of $30dBm$.

We first record how the charging power varies with the charging distance. From Figure 2, it can be observed that the received charging power decreases monotonically with the charging distance. For different charging distances, we also record the charging time by which the voltage reaches $2V$ from zero. As indicated in Figure 2, the charging time from 0 to $2V$ increases monotonically with the increasing relative distance.

Thus, it can be concluded that in spite of the difference among different charging models, there always exists a negative correlation between the charging power and distance, or in other words, a positive correlation between the time of charging and

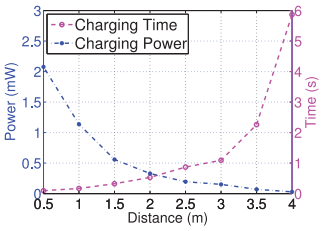

Fig. 2. Charging power and charging time.

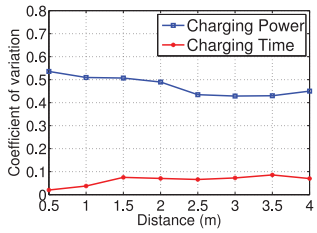

Fig. 3. Coefficient of variation.

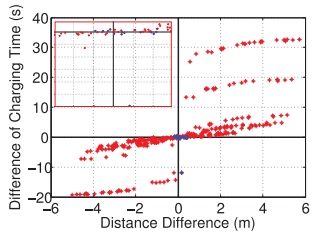

Fig. 4. Measurement unreliability.

distance. While it is costly to measure the exact charging power at the low-cost and tiny sensor node, we can alternatively compute the charging time by monitoring voltage of the capacitor by the available differential comparators and the RTC. Thus, for our TOC design, we utilize the simple fact that the node with a longer charging time is farther away from the charger, leading to the positive correlations between the charging time and charging distance to localize individual nodes.

Besides the ease of measurement, there are other benefits of utilizing TOC. The existing sequence-based localization methods, such as TOA, AOA, and TDOA, usually require highly accurate measurements. For example, TOA [Savvides et al. 2001a] needs precise measurements of time, and AOA [Niculescu and Badrinath 2003] requires accurate measurements of angle. However, for our TOC design, we utilize the *accumulative* charging process in a period of time, which makes it more robust and resilient to the *instantaneous* fluctuations of wireless charging power.

To verify the stability and robustness of using time of charging over instantaneous metrics such as charging power, we conduct experiments on our WISP-based testbed. We randomly place six sensor nodes and a charger in an outdoor parking lot for multiple topologies and record charging curves of each node. Charging time and power are then calculated based on the charging curve. Figure 3 shows the coefficient of variation of charging power and charging time versus different charging distances. From Figure 3, we see that the coefficient of variation of charging power is always higher than 0.4, whereas the coefficient of variation of charging time remains below 0.1. Since the coefficient of variation is a normalized measure of dispersion of a probability distribution, the results in Figure 3 validate the robustness of using time of charging over charging power.

Furthermore, in the experiment, we also examine the occurrence frequency of occasional charging time fluctuations. During each stop of the charger, we calculate the difference of charging time as well as the difference of charging distance for all node pairs and map them in Figure 4. From Figure 4, we find that the majority of points are located in the first quadrant and the third quadrant, which further proves the positive correlation between the charging time and distance. In Figure 4, points located in the second quadrant and the fourth quadrant are marked in blue (also shown in a zoomed-in figure in the upper-left corner). From the results, we can see that all blue dots are located near the axis $x = 0$. This means that although charging time fluctuations occur occasionally, they are within a very narrow band. This is consistent with the intuition that such fluctuations are more likely to happen when two nodes share similar charging distances from the reader. Such a property makes it possible to directly filter out the fluctuated measurements even when such measurement error happens occasionally. In Section 5, we will discuss a simple yet effective solution to resolve such occasional charging time fluctuations.

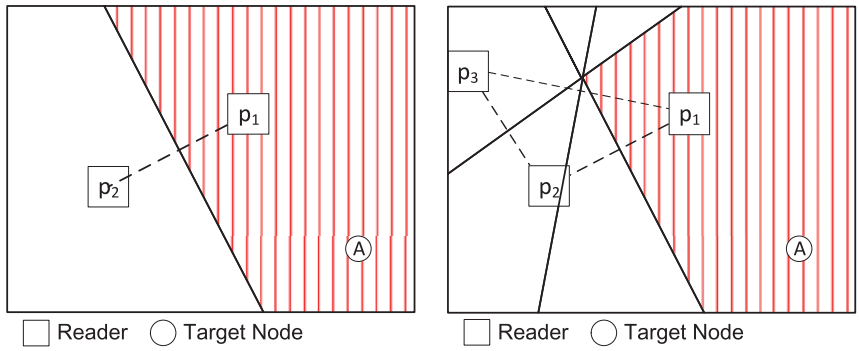

(a) Feasible region after two stops of the charger (b) Feasible region after three stops of the charger

Fig. 5. Internode division.

3. BASIC TOC DESIGN

In this section, we elaborate on the basic TOC design, which consists of *Internode Division* and *Interarea Division*.

3.1. Settings

Consider N wireless rechargeable nodes randomly deployed in an area of size S. We define the feasible region for each node i as the minimal region, where node i is guaranteed to be inside. At the beginning of the localization process, the feasible region of each target node is simply the whole region S. Moreover, in TOC, we set the center of gravity of the feasible region as the estimated location of the target node. Intuitively, it is necessary to narrow down the feasible region in order to obtain an accurate localization result.

To locate target nodes, one charger moves freely within the area. The charger is able to decide where to stop and turn its radio on to charge the nearby sensors. Each sensor responds to the charger once its voltage reaches a threshold. And each sensor will return to the fully discharged state before the next recharging due to the workload and highly limited energy capacity. For example, the discharge rate is around $10^{-3}W$ for a typical WISP node equipped with a $10\mu F$ capacitor, and the discharging time is around 100ms [Ransford et al. 2011], which is considerably short. We denote the charging time for reaching a fixed voltage threshold as the charging time for each node.

Generally, different charger stop positions make the charging time vary for each sensor. In this part, we show that even a random stop of the charger could greatly reduce the feasible region of each sensor. In the next section, we will further discuss how to optimize the charger stop positions for better localization performance.

For the purpose of introducing the key idea, in this section we assume the TOC readings at individual nodes are strictly negatively correlated with their distances to the charger. In Section 5, we will relax this assumption and discuss how to deal with occasional TOC reading flips in practice.

3.2. Internode Division

We first illustrate the idea of how to narrow down the feasible region of each node individually with continuous stops of the charger, which is named *Internode Division*.

In Figure 5(a), target node A is to be localized, denoted by numbered circles. The charger randomly stops at two different positions, which are denoted by numbered squares, that is, p_1 and p_2. Since node A is closer to p_1, it would have a shorter charging

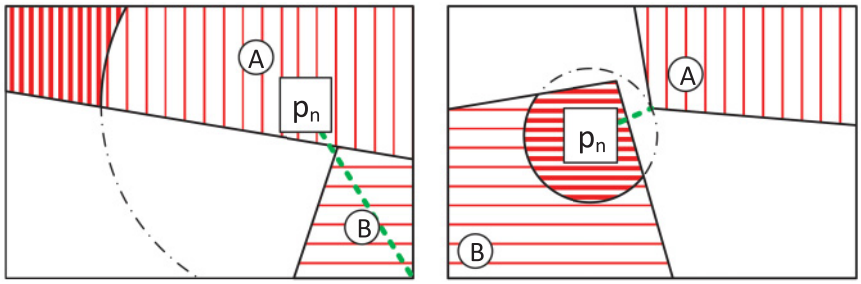

(a) Case 1 (b) Case 2

Fig. 6. Interarea division.

time for charger position p_1 than p_2. Therefore, we can infer that node A must lie on the right of the perpendicular bisector of these two stop positions.

Suppose the charger stops at another position, denoted by p_3 as in Figure 5(b). We can draw another two perpendicular bisectors and further narrow down the feasible region (i.e., the shaded area) of node A.

Denote $t(A, p)$ as the time of charge for node A when the charger stops at position p, and $d(p_i, p_j)$ as the Euclidean distance between two points p_i and p_j. This property can be summarized in the following lemma.

LEMMA 3.1. *Consider an arbitrary pair of charger stop positions, p_1 and p_2, and one node A. If $t(A, p_1) \leq t(A, p_2)$, then $d(A, p_1) \leq d(A, p_2)$, and vice versa.*

It can be proved that, by *Internode Division*, all feasible regions remain as convex polygons. In addition, we notice that the increasing number of stop positions will generate an exponentially increasing number of perpendicular bisectors. Specifically, the nth stop of the charger generates $n - 1$ perpendicular bisectors. And a total of $\frac{n(n-1)}{2}$ perpendicular bisectors will exist after n times of stops, which will divide the original feasible region into $\frac{(n^4-2n^3+3n^2-2n+8)}{8}$ pieces at most. Thus, it is expected that *Internode Division* will be very effective to narrow down the feasible regions of all sensors simultaneously. According to our simulations, even with random charger stops, the area of feasible region of one node can be narrowed down to 7.8% of the original region after only five stops of the charger.

3.3. Interarea Division

In this part, we show how to further narrow down the feasible region obtained from *Internode Division* by utilizing the Time of Charge difference of each pair of sensors for the same charger position. The novel idea is that each node, which may not have been accurately localized, can help to narrow down the feasible regions of its peers.

We explain the idea by a simple example. Suppose node A and node B are distributed in an area with their initial feasible regions denoted by R_A and R_B, respectively, as shown in Figure 6. The charger stops at p_n to charge A and B simultaneously. First, if p_n is within the feasible region of A as shown in Figure 6(a), as the charging time of A is shorter than that of B, we can determine that the feasible region of A should be inside the circle centered at p_n (i.e., the dashed dotted line) with radius equal to the farthest distance between p_n and R_B (i.e., the dashed line). However, if p_n is within the feasible region of B as shown in Figure 6(b), as the charging time of A is still shorter than that of B, we can infer that the feasible region of B should be outside the circle centered at p_n with radius equal to the shortest distance between p_n and R_A.

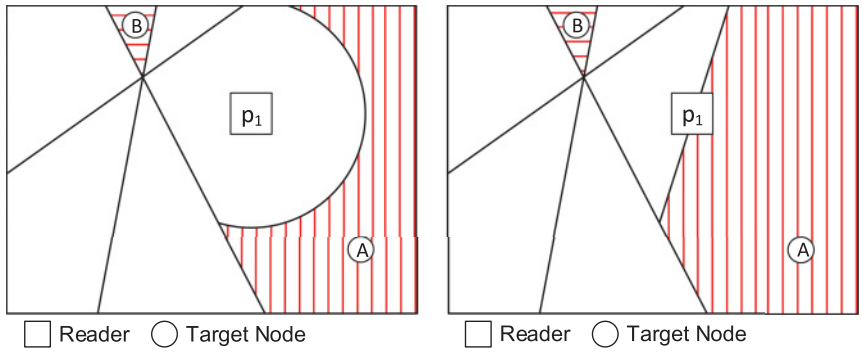

(a) Feasible regions after three stops of the charger (b) Feasible regions after the convex fix

Fig. 7. Interarea division.

Denote that $d_{max}/d_{min}(\cdot, \cdot)$ represents the maximal/minimal distance function. The previous properties are summarized in the following lemma.

LEMMA 3.2. *Consider an arbitrary pair of nodes, A and B, with initial feasible region as R_A and R_B, respectively. Suppose the charger stops at p_r and the charging time of node A is less than that of node B; then $\forall p_A \in R_A, d(p_A, p_r) < d_{max}(R_B, p_r)$, and $\forall p_B \in R_B, d(p_B, p_r) > d_{min}(R_A, p_r)$.*

To further understand Lemma 3.2, let us consider the example depicted in Figure 7(a). If we find that the charging time of node B is less than that of node A when the charger stops at the first position p_1, then based on Lemma 3.2, we draw a circle centered at p_1 with radius $r = d_{min}(p_1, p_B)$ to further narrow down the feasible region of node A, which is shown in Figure 7(a). Note that although the original feasible regions after *Interarea Division* may not remain to be convex polygons, for the ease of analysis, we can replace them by their corresponding convex hulls, which are good approximations of the original shape (see Figure 7(b)).

4. EXTENDED TOC DESIGN

Based on the ideas of Basic TOC, in this section we show how to localize the target nodes more effectively by planning the charger stop positions. We first present an optimal solution for the scenario where a single node is required to be localized. Then we extend the solution to solve the general multisensor scenario with a guaranteed approximate ratio.

4.1. Optimal Region Cutting for One Node

In this part, we introduce an optimal cutting algorithm that divides a feasible region with a single line. The charger will be able to decide the optimal stop sequence with this algorithm. Moreover, the results will provide insights to develop a solution for the more general scenario with multiple nodes.

4.1.1. Problem Definition. Consider an original feasible region R and the set of its vertices $V_R = \{v_1, v_2, v_3, v_4, v_5\}$ as shown in Figure 8. $d(R)$ represents one diameter among the feasible region R. After another stop of the charger, one additional perpendicular bisector can be generated as the cutting line $l = (p_i, p_j)$, where p_i and p_j are intersections with the edges of R. And this perpendicular bisector divides the region R into two subregions R_1 and R_2. Since the longest diameter of R_1 and R_2 is positively related to the localization error, the optimal cutting problem aims to find the cutting

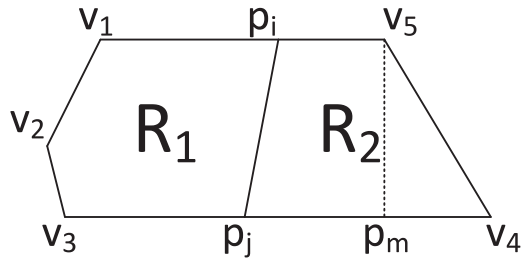

Fig. 8. Original feasible region R.

strategy p_i and p_j so as to minimize the longest diameter of the resultant subregions. Mathematically, the problem can be written as

$$Min\{E_{max}\}, \tag{1}$$

where E_{max} is termed as the *Maximal Localization Error* and

$$E_{max} = Max\{d_{max}(R_1), d_{max}(R_2)\}. \tag{2}$$

4.1.2. Preliminaries. In order to transform the problem into a more concrete and simplified form, we introduce the following lemma and its corollary.

LEMMA 4.1. *With optimal cutting, the maximal localization error can only be achieved by one pair of vertices at either R_1 or R_2. Moreover, such a pair of vertices cannot be two neighboring vertices of the original region R.*

PROOF. The first half is not difficult to prove by contradiction. Hence, we only show the idea of how to prove the second half. Take Figure 8 as an example. Assume that $l = (p_i, p_j)$ is the optimal cutting and the edge (v_1, v_2) has the longest distance. However, we can always construct another cutting strategy by moving either p_i or p_j, which reduces the maximal localization error. Thus, the assumption is violated, which completes the proof. □

Through Lemma 4.1, we can prove that one end of the longest distance among two cutting regions must be the cutting point (i.e., p_i or p_j). Then, Equation (2) can be reduced as

$$E_{max} = Max\{d_{max}(p_i, V_R), d_{max}(p_j, V_R)\}. \tag{3}$$

Formally, we have Corollary 4.2 as follows:

COROLLARY 4.2. *The optimal cutting problem is equivalent to the problem of finding a point p_i that minimizes $d_{max}(p_i, V_R)$.*

Therefore, for minimizing the longest distance of the two cutting regions, we only need to find a point p_i on the edges of R, which has the minimal distance to the farthest vertex.

4.1.3. Algorithm Design. Intuitively, there are an infinite amount of points on the edges of R. To reduce the search space for p_i, first we introduce Theorem 4.3, which makes our optimal cutting algorithm practical.

THEOREM 4.3. *For the original region R, we define two sets of points:*

(1) *For any pair of vertices of R, such as v_i and v_j, define $\{p_{ij}\}$ as the set of points that belong to the edges of R and satisfy $d(p_{ij}, v_i) = d(p_{ij}, v_j)$. This means points in $\{p_{ij}\}$ have the same distance between vertex v_i and v_j.*

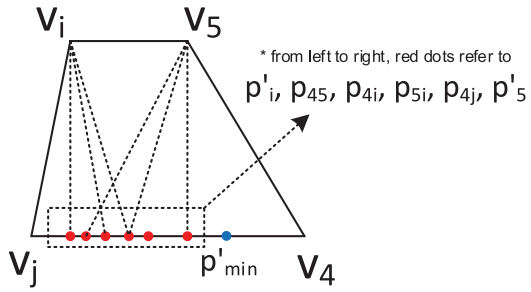

Fig. 9. Proof of Theorem 4.3.

(2) *For any edge $l(v_i, v_j)$, define $\{p_m\}$ as the set of points that belong to the edge $l(v_i, v_j)$ and satisfy $l(p_m, v_k) \perp l(v_i, v_j)$, where $v_k \in V_R$ and $v_k \neq v_i, v_j$. This means points in $\{p_m\}$ are the perpendicular foot of any vertex on the edges of R.*

Then $Min\{d_{max}(p_i, V_R)\}$ must be among the finite set composed of the previous two kinds of points.

PROOF. Consider the segmented region R_2 in Figure 8. For the sake of presentation, we change the name of p_i, p_j to v_i, v_j, respectively, and the updated R_2 is shown in Figure 9, where $V_{R_2} = \{v_4, v_5, v_i, v_j\}$. Points defined in Theorem 4.3 are marked as red dots as $\{p_{45}, p_{4i}, p_{5i}, p_{4j}\} \bigcup \{p'_i, p'_5\}$ (i.e., $d(p_{45}, v_4) = d(p_{45}, v_5), d(p_{4i}, v_4) = d(p_{4i}, v_i), d(p_{5i}, v_5) = d(p_{5i}, v_i), d(p_{4j}, v_4) = d(p_{4j}, v_j), l(p'_i, v_i) \perp l(v_j, v_4), l(p'_5, v_5) \perp l(v_j, v_4)$). Let p'_{min} be the point that has the global minimal $d_{max}(p, V_{R_2}) = d(p'_{min}, v_i)$. It is obvious that $d_{max}(p'_{min}, V_{R_2})$ will continuously change when point p'_{min} is moving along the bottom line. Therefore, by moving the point p'_{min} rightward or leftward, we can make sure that $d_{max}(p, V_{R_2}) = d(p'_{min}, v_i)$ can be decreased until reaching points that satisfy the first condition of Theorem 4.3 for v_i and any other vertex. Note that when $p'_{min} = p'_i$, moving p'_{min} will no longer decrease the distance $d(p'_{min}, v_i)$. Thus, the second kind of points stated in Theorem 4.3 should also be included as the feasible set. □

ALGORITHM 1: *Optimal Cutting Algorithm*

```
1: Input: R
2: L ← ∅
3: for each edge of R do
4:    ComputeCandidateSet S = {p_ij} ⋃ {p_m}
5:    for each element of S do
6:       ComputeDistance d_max(p_k, V_R) where p_k ∈ S
7:    end for
8:    L = L ∪ Min{d_max(p_ij, V_R)}
9: end for
10: return L
```

Based on Theorem 4.3, the optimal cutting algorithm is illustrated in Algorithm 1. To find the optimal cutting, we first generate all candidate points p_{ij} and p_m, which either satisfies $d(p_{ij}, v_i) = d(p_{ij}, v_j)$ or $l(p_m, v_k) \perp l(v_i, v_j)$ on every edge of R. We then compute the distance between each candidate point and vertices of R. After, we put the point with the minimal value of maximal distance to vertices of R on each edge into set L. When the algorithm terminates, the line that connects points in L with the two minimal values is the optimal cutting line. Then the optimal charger stop position can

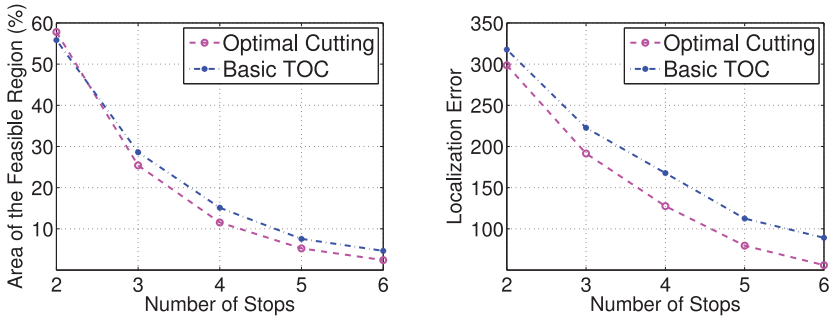

(a) Area of the feasible region (b) Localization error

Fig. 10. Optimal cutting versus Basic TOC (single node).

Table I. Localization Error Improvement with Optimal Cutting

Number of stops	2	3	4	5	6
Improvement (%)	5.99	14.02	23.92	29.20	37.31

be obtained through the fact that the optimal cutting line should be the perpendicular bisector of the optimal stop position and the previous stop position.

4.1.4. Complexity Analysis. Denote the number of vertices of R as n_v and the number of edges of R as n_e, and we have $n_v = n_e = |V_R|$. Since $\{p_{ij}\}$ and $\{p_m\}$ are nonunique among different edges of R, we need to iterate through all edges in R in the optimal algorithm, and consequently, there are n_v choices. For each edge, we have at most $({n_v}^2) + (n_v - 2)$ candidate points and we have to compute $d_{max}(p, V_R)$ for $[({n_v}^2) + (n_v - 2)] \cdot n_v$ times. Therefore, the overall algorithm complexity is $O(n_v^4)$.

4.1.5. Algorithm Performance and Insights. To evaluate the performance of the optimal cutting algorithm, we conduct the simulation where the charger chooses stop positions by the optimal cutting algorithm, and then compare the performance with Basic TOC where the charger stops randomly.

From Figure 10, we can see that both the area of the feasible region and the localization error decrease with the increasing number of stops of the charger. In addition, the optimal cutting algorithm outperforms the random stop of the charger in Basic TOC in terms of both the feasible region area and the localization error. Table I summarizes the percentage improvement of the optimal cutting algorithm in localization error compared with Basic TOC. For example, after six stops of the charger, the localization error decreases by 37.31%.

Furthermore, by examining the results of the optimal cutting algorithm, we observe that the optimal cutting algorithm tends to cut off the longest diagonals of the feasible region. Specifically, the first or second longest diagonals are always being cut off for all simulation runs. Such insights allow us to design a more efficient approximation algorithm with performance guarantees in the next section.

4.2. Cutting for Multiple Nodes

The optimal cutting algorithm for the single-node case divides the feasible region with minimized maximal localization error under the polynomial complexity. However, if the multisensor scenario is taken into consideration, we can no longer only focus on the feasible region of one node. Moreover, the *Interarea Division* makes the computation even more complicated as the overall complexity of the optimal single cut solution is already $O(n_v^4)$. To handle this problem, in this part we first extend the optimal region

cutting algorithm for one node to an approximation algorithm that is proved to be more general. Then, inspired by the approximation solution for the single-node case, we introduce an approximation solution for the multinode scenario with a provable approximation ratio.

4.2.1. Extension of the Optimal Design. The main idea of our approximation algorithm is that by cutting more long diagonal lines of the original polygon, we are more likely to minimize the maximal distance of two subdivided regions.

ALGORITHM 2: *Approximated Optimal Cutting Algorithm*

1: **Input**: R
2: $L \leftarrow \emptyset$
3: Compute $D = \{\{d(v_i, v_j), v_i, v_j\}\}$, $v_i, v_j \in V_R$
4: Sort D based on $d(v_i, v_j)$
5: **repeat**
6: $\quad L = L \cup Max\{D\}$
7: $\quad D = D - Max\{D\}$
8: **until** $StabbingLineSegments(L) == 0$
9: **return** L

The process of the approximation algorithm is depicted in Algorithm 2. First, we enumerate all pairs of vertices of the original polygon and calculate and sort diagonal lines between each pair of nodes in nonincreasing order (Lines 3 to 4). Then we iterate through the sorted diagonal lines and check whether there exists a line that intersects with all previous longest diagonals (Lines 5 to 8). To obtain a line that intersects a set of diagonal lines, we utilize the $StabbingLineSegments(L)$ function, which is a well-studied topic in computational geometry [Edelsbrunner et al. 1982; Katz et al. 2005]. The function returns false if the line does not exist. Essentially, Algorithm 2 tries to continuously cut the longest diagonal lines until it cannot cut any more. Once the algorithm terminates, we can decide the corresponding charger stop position that can generate a perpendicular bisector that intersects the top $|L|$ longest lines within region R.

Given the number of vertices, n_v, the computation complexity of enumerating and sorting is $O(n_v^3 lgn_v)$. A widely accepted computation complexity for finding stabbing lines from a set of lines is $\Theta(nlgn)$ [Edelsbrunner et al. 1982], where n is the number of lines.

To quantitatively analyze the performance of our proposed approximation algorithm, we have the following theorem.

THEOREM 4.4. *Let l_{opt} be the optimal dividing line calculated from Algorithm 1 and $\{l_{app}\}$ be an infinite set of all feasible lines calculated from Algorithm 2. We have $l_{opt} \in \{l_{app}\}$.*

PROOF. We prove the theorem by contradiction. If $l_{opt} \notin \{l_{app}\}$, either $l(v_i, v_j)$, $d(v_i, v_j) = Min\{L\}$ has not been cut off or $d(v_i, v_j) = Max\{D\}$ has been cut off. If $l(v_i, v_j)$ with $d(v_i, v_j) = Min\{L\}$ exists in the segmented regions, we can replace the l_{opt} by any element in the set $\{l_{app}\}$. If $l(v_i, v_j)$ with $d(v_i, v_j) = Max\{D\}$ has been successfully cut off in l_{opt}, $Max\{D\}$ must be an element of L. Therefore, we must have $l_{opt} \in \{l_{app}\}$. □

The insight of Theorem 4.4 is that the result of the optimal cutting algorithm is a special case among the approximation results. Based on Theorem 4.4, we have $Min\{L\} \geq Min\{E_{max}\} \geq Max\{D\}$. In other words, we expand the optimal result in Section 4.1 to the range between $Min\{L\}$ and $Max\{D\}$. Consequently, the approximation ratio of our algorithm $\rho = Max\{Min\{L\}\}/E_{opt} \leq Min\{L\}/Max\{D\}$.

4.2.2. Cutting for Multiple Nodes. In a multisensor scenario, it is intrinsically difficult to obtain the optimal stop position of the charger due to the high complexity in both spatial and temporal dimensions. Thus, we focus on a heuristic design that extends the approximation algorithm for a single node with guaranteed localization performance.

ALGORITHM 3: *Multisensor Localization Algorithm*

Input: $\{R_k\}$, $k \in [1, N]$
$L \leftarrow \emptyset$
for each $k \in [1, N]$ **do**
  Compute $D = \{\{d(v_i^k, v_j^k), v_i^k, v_j^k\}\}$, $v_i^k, v_j^k \in P_R^k$
end for
Sort D based on $d(v_i^k, v_j^k)$
repeat
  $L = L \cup Max\{D\}$
  $D = D - Max\{D\}$
until $StabbingLineSegments(L) == 0$
return L

Algorithm 3 illustrates the localization process for the multinode case. The main idea is to cut more diagonals of all feasible regions every time with joint consideration of all nodes. Denote the number of nodes as N; we first calculate distances among vertices of all nodes and sort them in set D. After that, we gradually put elements of D into set L according to the descending order of its length similar to Algorithm 2. Therefore, it can be guaranteed that the longest $|L|$ lines among all feasible regions will be cut at each step.

This way, we approximately minimize the maximal distance among all target nodes in the network. It can be proved that the approximation ratio of the multinode algorithm is $\rho = Min\{L\}/Max\{D\}$. In other words, our approximation algorithm guarantees that, after cutting, the longest distance among feasible regions will be less than ρ times of the optimal solution.

Recall that in Basic TOC, we can draw $n - 1$ perpendicular bisectors at the nth stop of the charger. Therefore, to generate the cutting line computed in Algorithm 3, we have $n - 1$ candidate stop positions. To make full use of these perpendicular bisectors, among these candidates we choose the optimal stop position that minimizes the average localization error.

5. DISCUSSION

We summarize the costs and limitations of TOC and discuss the countermeasures in this part.

In order to utilize TOC, we need to be able to localize the charger. However, in the majority of mobile charging scenarios where the charger is carried by vehicles (e.g., robots/drones), accurate positioning is achievable through add-on devices like GPS. In indoor environments, positioning of the mobile charger can be accomplished through numerous localization approaches such as Simultaneous Localization and Mapping (SLAM) [Durrant-Whyte and Bailey 2006] and device-free indoor localization methods [Popleteev 2013; Xiao et al. 2013].

Another cost of TOC localization is the charging delay and charger's movement delay. However, according to our experimental results shown in Figure 2, the charging time of RFID-based rechargeable sensor nodes is less than 8 seconds even when the charger is 4 meters away. We believe the charging delay could be further reduced in the near future with the development of new antennae and low-power digital design technology. Due to the nonnegligible moving delay, TOC does not apply to mobile target

localization. Specifically, the previous charging sequences will become invalid when nodes move between two stops of the charger. Therefore, we cannot combine TOC results at different stop locations and divide the feasible region efficiently.

In previous sections, we introduced both Basic TOC and advanced TOC under the assumption that the charging time is strictly negatively correlated with the charging distance. In this section, we discuss the impact of occasional charging time flips in TOC design and elaborate on solutions for dealing with such cases.

Typically, the flips of charging times are mainly due to two major reasons. The first reason is the radio irregularity and interference in wireless charging. Similar to wireless communications, such radio irregularity is caused by the nonisotropic properties of the propagation media and the heterogeneous properties of devices [Zhou et al. 2004]. The second reason is the measurement errors. Such errors are caused by measurement noises and random wireless communication errors such as packet loss and collisions. Both of these two reasons could lead to the change of instantaneous charging powers on WRSN nodes and cause the flips of charging times.

However, since TOC compares the charging time differences among individual nodes instead of instantaneous charging power, it is more robust and resilient to instantaneous charging power fluctuations caused by various factors. For example, through our empirical measurement, the coefficient of variation of charging power is four times as high as that of charging time.

To deal with occasional potential charging time flips, in our design, we propose a simple yet effective solution. Assume the charging time of node A is T_i and T_j when the charger stops at location p_i and p_j, respectively. We divide the feasible region of node A only when $|T_i - T_j| > \varepsilon/\sqrt{(\min\{T_i, T_j\})}$ in Section 3.2 and Section 3.3. Rationale of the equation is based on two observations: (1) the probability of flip is low if there exists a relatively large gap between charging times of two nodes, and (2) for a fixed difference between charging times of two pairs of nodes, flip is more likely to happen in the pair of nodes that is closer to the charger. We term ε as the unreliability threshold and empirically choose its value for different WRSN platforms. For example, for our WRSN testbed used in Section 6.1, we set ε as 0.6 based on the offline measurement results in Figure 4. Essentially, TOC with a larger ε is able to tolerate more severe charging power fluctuations as well as greater device diversity although it leads to slower localization of the nodes. In Section 6.5.4, we will further investigate the localization performance of TOC under different ε values.

6. PERFORMANCE EVALUATION

In this section, we first evaluate the performance of TOC through experiments. Large-scale simulations are further proposed in Section 6.3 and Section 6.4. In Section 6.5, we illustrate the impact of system parameters including the number of sensors, the node distributions, and the measurement error.

6.1. Experimental Evaluation

We first evaluate the TOC design on our WRSN testbed with six rechargeable sensor nodes.

6.1.1. Experimental Settings. During the experiment, six WISP nodes equipped with patch antennae (gain = 6.1dBi) are randomly distributed in an area of $15m * 15m$ (shown in Figure 11). An EPC C1G2 RFID reader stops at different locations to charge all nodes. The charger works at the frequency of 915MHz with the maximum transmission power of 30dBm. At each stop position, it wirelessly charges all nodes, continuously sends query commends, and accurately records the time of the first response from each node. Nodes will reply to the charger once it is charged to 1.9V. Without any prior

Fig. 11. Experimental area.

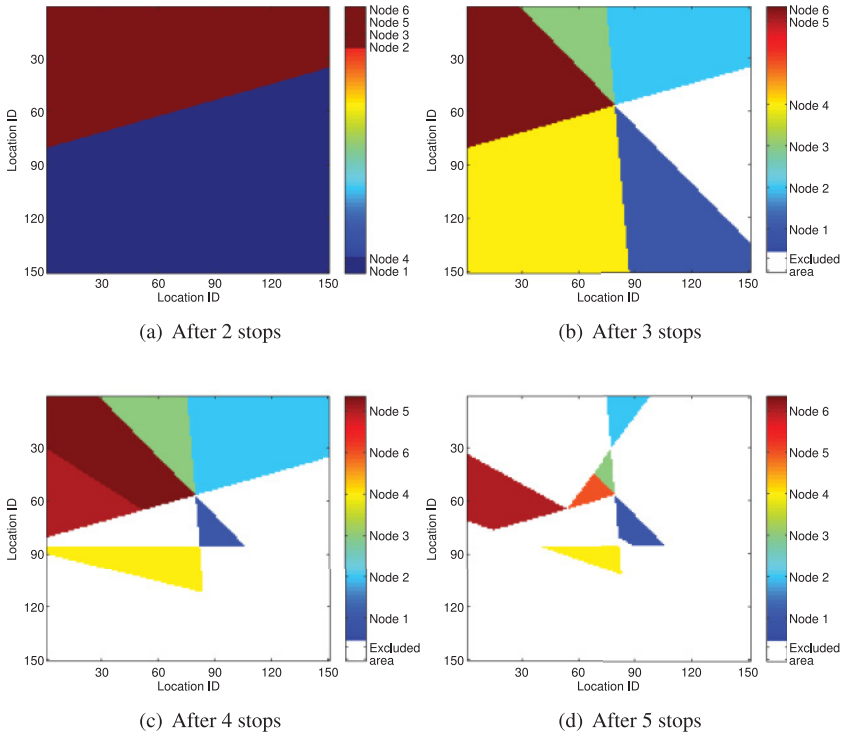

(a) After 2 stops (b) After 3 stops

(c) After 4 stops (d) After 5 stops

Fig. 12. Feasible region after each stop of the charger.

knowledge, we randomly choose the first two stop positions, then calculate the following stop positions based on our extended TOC design in Section 4.2. The localization process terminates when the total number of stops reaches five.

6.1.2. Experimental Results. Figure 12 shows how the feasible regions of all nodes evolves along with each stop of the charger, and the summarized localization results are listed in Table II.

From Table II, we can see that after three stops of the charger, 80% of the original area is excluded and the mean localization error decreases to less than 3m. After five stops of the charger, the average localization error has been reduced to 0.81m. Specifically, Figure 13 further shows the feasible regions and localization errors for each node after

Table II. Experimental Results

Number of stops	2	3	4	5
Area of feasible region (%)	47.97	20.51	10.84	2.78
Mean localization error (m)	3.82	2.95	1.82	0.81

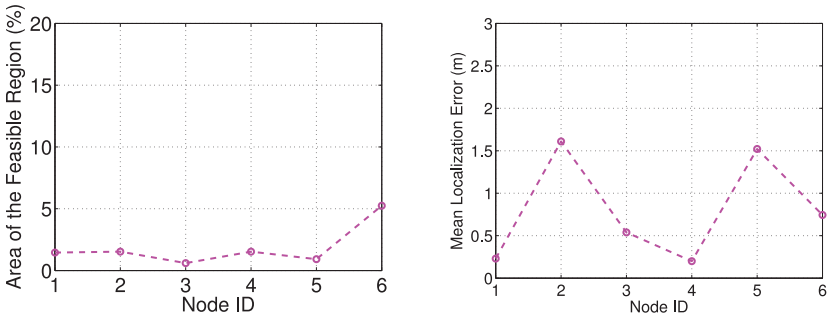

(a) Area of feasible region (%) (b) Localization error (m)

Fig. 13. Localization results among different nodes.

Table III. Default Simulation Parameters

Parameters	Description
Field area	$100m \times 100m$
Number of stops	6
Number of target nodes	100
Target node Ddistribution	Uniform distribution
Statistics	Feasible region; localization error
Random seed	100 runs

five stops of charger. From Figure 13, we find that all six nodes achieve good localization performance at around 1m and there is a small variation among different nodes. Since almost no flips of charging times can be observed on our testbed, we directly set the unreliability threshold ϵ as 0 during the experiment. In fact, if we increase ϵ from 0 to 1, around 17% cutting probabilities will be filtered, which will increase the localization error instead.

6.2. Simulation Settings

In addition to experiment evaluation, we conduct large-scale simulation to evaluate the performance of the Basic TOC, followed by the performance comparison between the Basic TOC and the Extended TOC. Default simulation parameters are shown in Table III. Note that due to the positive relationship between the charging distance and charging time, we do not need to specify the charging model and perform cutting only based on binary comparison results of each pair of nodes. We adopt the percentage area of the feasible region and the localization error as two metrics to evaluate localization performance. The percentage of the feasible region refers to the ratio of segmented area after each stop over the area of the original feasible region. The localization error is defined as the distance between the estimated position and the real location of the sensor. In addition, we also calculate the standard deviation of localization error among different sensors.

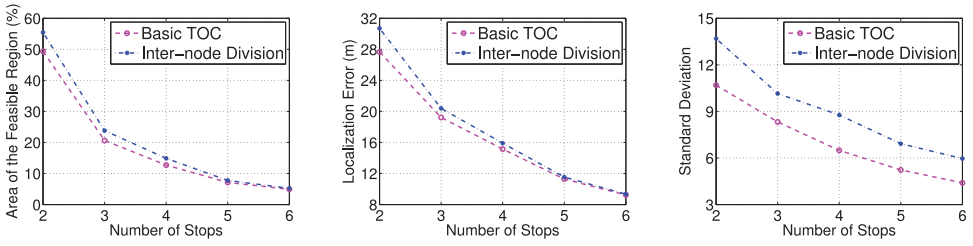

(a) Area of the feasible region (b) Mean localization error (c) Standard deviation of localization error

Fig. 14. Localization result of the Basic TOC (number of nodes = 100).

Table IV. Decrease of Area of the Feasible Region

Number of stops	2	3	4	5	6
Gain (%)	11.02	13.28	14.71	8.25	6.12

Table V. Decrease of Localization Error

Number of stops	2	3	4	5	6
Gain (%)	9.90	5.74	4.72	2.17	1.07

6.3. Performance of Basic TOC

In order to show the effectiveness of Basic TOC, we first compare the localization performance of the purely *Internode Division* approach with Complete Basic TOC, which combines *Internode Division* and *Interarea Division*. From Figure 14(a) and Figure 14(b), we can see that Complete Basic TOC does achieve better performance in terms of both the area of feasible region and the mean localization error. Table IV and Table V summarize the percentage gain of the *Interarea Division*. From Table IV and Table V, we find that the percentage gain of the *Interarea Division* decreases as the charger stops for more times. This is because the area of the feasible regions of nodes decreases quickly along with the number of charger stops, which makes the interarea division happen less frequently.

In Figure 14(c) and Table VI, we examine the standard deviation of localization error among different nodes. From Figure 14(c), we can see that the Complete Basic TOC provides a significantly smaller standard deviation than that of the purely *Internode Division*. For example, after the fourth stop of the charger, the standard deviation gain is as high as 29.6%. Results of Figure 14(c) and Table VI well support the effectiveness of *Interarea Division,* which utilizes the well-positioned nodes to help localize other related nodes so that the error deviation through the network can be kept at a lower level.

6.4. Extended TOC Versus Basic TOC

This section illustrates performance of the Extended TOC over the Basic TOC. To qualitatively analyze localization performance, we also plot the optimal results through exhaustive search, in which at each step, the charger selects the stop position for minimizing the mean localization error over the network.[1]

In Figure 15(a) and Figure 15(b), by optimizing the charger stop positions, the Extended TOC is able to reduce both the area of feasible regions and mean localization errors. It can be seen that the localization error decreases monotonically to around

[1]Due to the exponential growth of computation overhead, candidate stop locations are chosen every $g = 10m$ in the exhaustive search.

Table VI. Decrease of standard deviation of localization error

Number of stops	2	3	4	5	6
Gain (%)	21.91	18.03	26.00	24.42	26.17

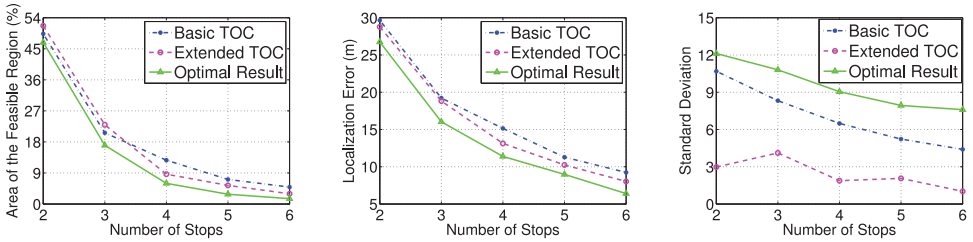

(a) Area of the feasible region (b) Mean localization error (c) Standard deviation of localization error

Fig. 15. Extended TOC versus Basic TOC (number of nodes = 100).

Table VII. Percentage Gain of the Mean Localization Error

Number of stops	2	3	4	5	6
Extended TOC (%)	2.97	2.09	13.33	9.27	13.16
Optimal result (%)	9.81	16.58	24.84	20.47	30.70

$8m$ after six stops. The detailed percentage gain of the mean localization error of both Extended TOC and the optimal results is shown in Table VII. For example, after four stops of the charger, the mean localization error of the Extended TOC is 13.33% less than the result of the Basic TOC (13.13m vs. 15.15m), and the optimal result owns a 24.84% decrease (11.39 vs. 15.15m). Comparing with the optimal results, we find that the Extended TOC offers a fairly good localization performance with computation time decreased by two orders of magnitude (18s vs. 2,031s).

In Figure 15(c), it is interesting to observe that the Extended TOC owns the fewest standard deviations of localization error, whereas the optimal results are larger than both the Basic TOC and the Extended TOC. By analyzing the optimal results, we find that quite often the optimal solution may have to sacrifice the localization error variance for the minimal localization error. Therefore, from Figure 15(c), we can see that the Extended TOC achieves a good balance between average localization error and variation.

6.5. Impact of System Settings

We examine the impact of sensor number, increasing number of stops of the charger, sensor distributions, and measurement errors in this part.

6.5.1. Impact of the Sensor Number. We vary the node number from 100 to 500 in the field sized $100m \times 100m$ and compare the localization performances of both Basic TOC and Extended TOC. Figure 16 shows the average area of feasible regions, mean localization error, and their standard deviations. It can be observed that both Basic TOC and Extended TOC achieve a steady performance in terms of three metrics, which shows the scalability of our design. Specifically, we can see that although the Extended TOC has a similar average area of feasible regions as the Basic TOC's, it achieves a much smaller mean localization error over the Basic TOC. In most cases, the improvement of mean localization error is higher than 10%. In addition, the standard deviations of localization error of the Extended TOC is much lower than the Basic TOC's, which

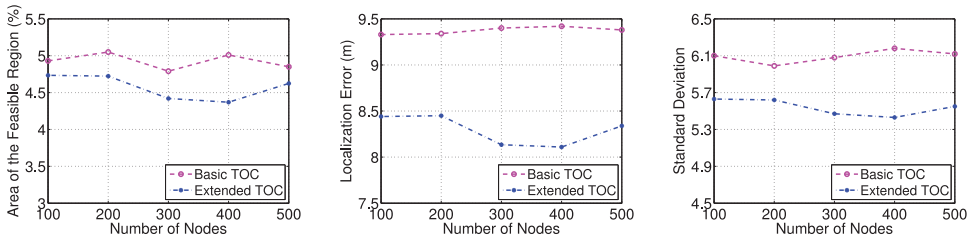

(a) Percentage area of the feasible region (b) Mean localization error (c) Standard deviation of localization error

Fig. 16. Impact of the number of target nodes (number of stops = 6).

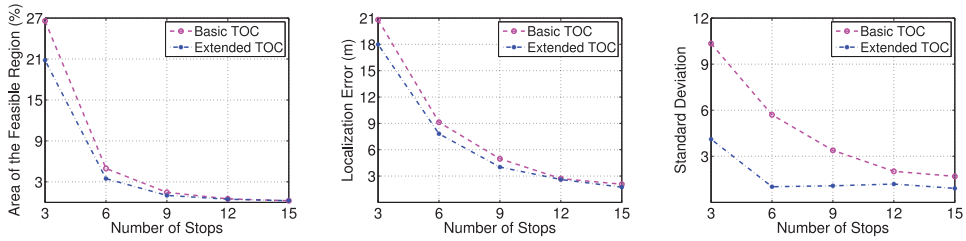

(a) Percentage area of the feasible region (b) Mean localization error (c) Standard deviation of localization error

Fig. 17. Impact of the number of stops (number of nodes = 6).

can be explained as we jointly sort distances among different nodes and cut off longer diagonals with a global consideration.

6.5.2. Impact of the Number of Stops. We evaluate the localization performances with various numbers of stops of the charger. Figure 17 shows the localization results of both Basic TOC and Extended TOC with up to 15 stops of the charger. From Figure 17, we can see that in both Basic TOC and Extended TOC, the mean localization error of nodes is less than $3m$ after 12 stops of the charger. Moreover, the Extended TOC outperforms the Basic TOC under each metric. For example, after 15 stops of the charger, the mean localization error of the Extended TOC ($1.73m$) is 16.28% less than that of the Basic TOC ($2.06m$).

6.5.3. Impact of the Sensor Distribution. In previous simulations, sensors are uniformly distributed. In this part, we evaluate localization performances of TOC with normal distribution and gamma distribution of sensors and compare them with the results under the uniform distribution. In normal distribution, we generate positions of nodes on both axis x and axis y with mean value $\mu = 50$ and variance $\sigma = 10$, while in gamma distribution, we set the shape parameter $k = 1$ and the scale parameter $\theta = 2$. Simulation results suggest that the Extended TOC is adaptive to two nonuniform distributions, as the mean localization error decreases with more stops of the charger and gaps among three different distributions are small (due to the space constraint, we omit related figures). However, when nodes are not uniformly distributed, localization performance of the Basic TOC becomes worse. For example, in Figure 18, we can see that the fluctuations of standard deviations of the Basic TOC are much greater than that of the Extended TOC. This is because the random stop of the charger in Basic TOC is not well suited for such nonuniform distributions. Figure 18 demonstrates that the proposed Extended TOC is highly effective and compatible with various distributions.

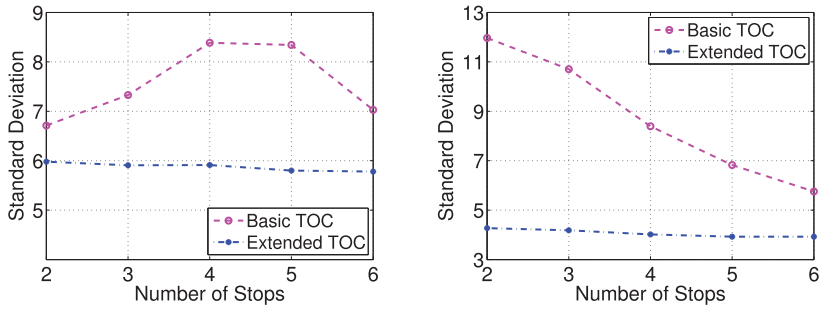

(a) Normal Distribution (b) Gamma Distribution

Fig. 18. Standard deviation of localization error.

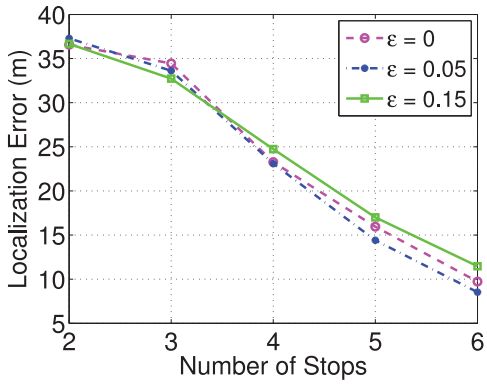

Fig. 19. Impact of the measurement error.

6.5.4. Impact of the Measurement Error. In this section, we evaluate localization performances of TOC with measurement error. In simulations, 100 nodes are randomly deployed in the field sized $100m \times 100m$. Measurement error obeys a normal distribution with zero mean and variance σ. For $\sigma = 0.4$, localization results under different measurement unreliability thresholds ε are shown in Figure 19.

From Figure 19, we can see that with a fixed measurement error, adopting a nonzero ε ($\varepsilon = 0.05$) enhances the localization performance. However, choosing an overly large ε ($\varepsilon = 0.15$) leads to TOC performance degradation. This is because with large ε, TOC divides the feasible regions of nodes less frequently as more cutting chances are filtered out by the overly large ϵ. Therefore, to obtain a satisfactory localization performance, we need to deliberatively decide the measurement unreliability threshold.

7. RELATED WORK

Many works have proposed to localize nodes in wireless sensor networks. Based on the underlying localization techniques, there are mainly two types of methods: range-based localization and range-free localization. Range-based localization methods such as GPS, AOA [Niculescu and Badrinath 2003], Sweeps [Goldenberg et al. 2006], SRIPS [Dil and Havinga 2011], and ArrayTrack [Xiong and Jamieson 2013] measure point-to-point distances or angles among sensor nodes and/or anchor nodes to compute per-node position. Although they tend to offer precise locations of nodes, they incur unfavorable costly additional hardware or environment profiling. Range-free localization methods [Zhong and He 2009; Römer 2003; Xu et al. 2011; Doherty et al. 2001], on the other hand,

Table VIII. Comparison of TOC with RSSI-Based Localization Techniques

Systems	Localization Time	Accuracy	Complexity	Cost	Pros	Cons
TOC	Non-instantaneous	Medium	Low	Low	Robust and resilient to environmental changes	Localization delay, localization of static targets
RF FP	Non-instantaneous	High	High	High	High accuracy, mobile targets localization	Onerous map calibration, anchor nodes, high computation overhead
RF modeling	Instantaneous	Low	Low	Medium	Simple and energy efficient	Anchor nodes, weak adaptability to multipath environment with interference

localize nodes based on their connectivity information or simple sensing of their relative positions. However, such kinds of localization systems need either several anchor nodes or precise event distributions, which makes them less effective for practical deployment.

Another category of localization algorithms is based on the Received Signal Strength Indication (RSSI) [Madigan et al. 2005; Youssef and Agrawala 2005; Lin et al. 2010; Chintalapudi et al. 2010; Constandache et al. 2009; Bahl and Padmanabhan 2000; Azizyan et al. 2009; Savvides et al. 2001b]. These algorithms can be further categorized into modeling-based methods [Constandache et al. 2009; Chintalapudi et al. 2010; Madigan et al. 2005; Lin et al. 2010; Savvides et al. 2001b] and fingerprinting-based (FP) methods [Youssef and Agrawala 2005; Bahl and Padmanabhan 2000; Azizyan et al. 2009]. The former create an RSS model of the entire network, while the latter leverage an RF fingerprint map through site surveying (a.k.a. war driving). However, due to the inherent variability in wireless signal propagation characteristics and the presence of severe multipath fading with multiple reflections, the relationship between RSSI and distance is extremely hard to model, limiting the accuracy of both model-based methods and fingerprinting-based methods. To further compare the performance of TOC with RSSI-based localization approaches, we summarize their key features in terms of localization time, accuracy, system complexity, cost, pros, and cons in Table VIII. The cost refers to the predeployment effort of the localization system. From Table VIII, we observe that TOC achieves better balance in terms of localization accuracy and cost over RSSI-based localization techniques. For example, RF fingerprinting approaches achieve high localization accuracy at the cost of complexity of algorithms (e.g., the heavy computational burden of the particle filter). Compared with RF modeling techniques, TOC exhibits better performance in a rich multipath environment with interference. However, it suffers from the localization time and cannot localize mobile targets.

Wireless power transfer technology has been adopted in many existing WRSNs. One representative example is the WISP, which harvests energy from the off-the-shelf commercial RFID reader [Sample et al. 2008]. After being first proposed in 2008, there have been many works on WISP-based WRSN [He et al. 2013; Shu et al. 2014b; Gummeson et al. 2010; Shu et al. 2014a; Fu et al. 2013].

Despite the diversity of work that has been done on both localization of sensor nodes and wireless rechargeable sensor networks, little work has been proposed on localization in WRSN. In this article, we adopt the fundamental charging principle and propose a TOC-based localization method. Our design is compatible with most wireless rechargeable sensor networks as well as wireless energy harvesting technologies. In addition, it avoids the limitations of range-based, range-free, and RSSI-based localization methods and does not rely on additional hardware, anchors, or generated events.

8. CONCLUSION

In this article, we study the problem of how to use the Time of Charge sequences of wireless rechargeable sensor nodes to localize themselves. We first identify the fundamental relationship between charging time and distance between nodes and the charger. Based on this principle, we propose two localization methods, Basic TOC and Extended TOC. In Basic TOC, the charger stops randomly in the field to charge nodes and divides their feasible regions iteratively. In Extended TOC, we further optimize the charger stop positions based on the estimated sensor locations so as to achieve higher localization accuracy. To verify our designs, we perform detailed performance evaluations through analysis and large-scale simulations. To the best of our knowledge, it is the first work designed for localization in wireless rechargeable sensor networks by purely using the Time of Charge sequences.

REFERENCES

A. E. A. A. Abdulla, H. Nishiyama, J. Yang, N. Ansari, and N. Kato. 2012. HYMN: A novel hybrid multi-hop routing algorithm to improve the longevity of WSNs. *IEEE Transactions on Wireless Communications* 11, 7 (2012), 2531–2541.

M. Azizyan, I. Constandache, and R. R. Choudhury. 2009. SurroundSense: Mobile phone localization via ambience fingerprinting. In *ACM Mobicom*.

P. Bahl and V. N. Padmanabhan. 2000. RADAR: An in-building RF-based user location and tracking system. In *IEEE INFOCOM*.

D. J. A. Bijwaard, W. A. P. van Kleunen, P. J. M. Havinga, L. Kleiboer, and M. J. J. Bijl. 2011. Industry: Using dynamic WSNs in smart logistics for fruits and pharmacy. In *ACM SenSys*.

X. Cao, J. Chen, Y. Zhang, and Y. Sun. 2008. Development of an integrated wireless sensor network micro-environmental monitoring system. *ISA Transactions* 47, 3 (2008), 247–255.

K. Chintalapudi, A. Padmanabha Iyer, and V. N. Padmanabhan. 2010. Indoor localization without the pain. In *ACM MobiCom*.

I. Constandache, S. Gaonkar, M. Sayler, R. R. Choudhury, and L. Cox. 2009. EnLoc: Energy-efficient localization for mobile phones. In *IEEE INFOCOM*.

B. Dil and P. J. M. Havinga. 2011. Stochastic radio interferometric positioning in the 2.4 GHz range. In *ACM SenSys*.

L. Doherty, K. S. J. Pister, and L. El Ghaoui. 2001. Convex position estimation in wireless sensor networks. In *IEEE INFOCOM*.

H. Durrant-Whyte and T. Bailey. 2006. Simultaneous localization and mapping: Part I. *IEEE Robotics Automation Magazine* 13, 2 (June 2006), 99–110.

H. Edelsbrunner, H. A. Maurer, F. P. Preparata, A. L. Rosenberg, E. Welzl, and D. Wood. 1982. Stabbing line segments. *BIT* 22, 3 (1982), 274–281.

L. Fu, P. Cheng, Y. Gu, J. Chen, and T. He. 2013. Minimizing charging delay in wireless rechargeable sensor networks. In *IEEE INFOCOM*.

D. K. Goldenberg, P. Bihler, Y. R. Yang, M. Cao, J. Fang, A. S. Morse, and B. D. O. Anderson. 2006. Localization in sparse networks using sweeps. In *ACM MOBICOM*.

J. Gummeson, S. S. Clark, K. Fu, and D. Ganesan. 2010. On the limits of effective hybrid micro-energy harvesting on mobile CRFID sensors. In *ACM MobiSys*.

L. He, Z. Yang, J. Pan, L. Cai, and J. Xu. 2012. Evaluating service disciplines for mobile elements in wireless ad hoc sensor networks. In *IEEE INFOCOM*.

S. He, J. Chen, F. Jiang, D. K. Y. Yau, G. Xing, and Y. Sun. 2013. Energy provisioning in wireless rechargeable sensor networks. *IEEE Transactions on Mobile Computing* 12, 10 (Oct. 2013), 1931–1942.

T. He, C. Huang, B. M. Blum, J. A. Stankovic, and T. Abdelzaher. 2003. Range-free localization schemes for large scale sensor networks. In *ACM MobiCom*. 81–95.

B. Karp and H. T. Kung. 2000. GPSR: Greedy perimeter stateless routing for wireless networks. In *ACM MobiCom*.

M. J. Katz, J. S. B. Mitchell, and Y. Nir. 2005. Orthogonal segment stabbing. *Computational Geometry* 30, 2 (2005), 197–205.

Y. J. Kim, R. Govindan, B. Karp, and S. Shenker. 2005. Geographic routing made practical. In *NSDI*.

K. Lin, A. Kansal, D. Lymberopoulos, and F. Zhao. 2010. Energy-accuracy trade-off for continuous mobile device location. In *ACM MobiSys*.

G. Liu, W. Yu, and Y. Liu. 2006. Resource management with RFID technology in automatic warehouse system. In *IEEE IROS*.

D. Madigan, E. Einahrawy, R. P. Martin, W.-H. Ju, P. Krishnan, and A. S. Krishnakumar. 2005. Bayesian indoor positioning systems. In *IEEE INFOCOM*.

D. Niculescu and B. R. Badrinath. 2003. Ad hoc positioning system (APS) using AOA. In *IEEE INFOCOM*.

T. C. Poon, K. L. Choy, H. K. H. Chow, H. C. W. Lau, F. T. S. Chan, and K. C. Ho. 2009. A RFID case-based logistics resource management system for managing order-picking operations in warehouses. *Expert Systems Applications* 36, 4 (2009), 8277–8301.

A. Popleteev. 2013. Device-free indoor localization using ambient radio signals. In *ACM UbiComp*.

B. Ransford, J. Sorber, and K. Fu. 2011. Mementos: System support for long-running computation on RFID-scale devices. In *ASPLOS*.

K. Römer. 2003. The lighthouse location system for smart dust. In *ACM MobiSys*.

A. P. Sample, D. J. Yeager, P. S. Powledge, A. V. Mamishev, and J. R. Smith. 2008. Design of an RFID-based battery-free programmable sensing platform. *IEEE Transactions on Instrumentation and Measurement* 57, 11 (2008), 2608–2615.

A. Savvides, C. C. Han, and M. B. Srivastava. 2001a. Dynamic fine-grained localization in ad-hoc networks of sensors. In *ACM MobiCom*.

A. Savvides, C.-C. Han, and M. B. Strivastava. 2001b. Dynamic fine-grained localization in Ad-Hoc networks of sensors. In *ACM Mobicom*.

Y. Shu, P. Cheng, Y. Gu, J. Chen, and T. He. 2014a. Minimizing communication delay in RFID-based wireless rechargeable sensor networks. In *IEEE SECON*.

Y. Shu, Y. (J.) Gu, and J. Chen. 2014b. Dynamic authentication with sensory information for the access control systems. *IEEE Transactions on Parallel Distributed Systems* 25, 2 (2014), 427–436.

J. Xiao, K. Wu, Y. Yi, L. Wang, and L. M. Ni. 2013. Pilot: Passive device-free indoor localization using channel state information. In *IEEE ICDCS*.

J. Xiong and K. Jamieson. 2013. ArrayTrack: A fine-grained indoor location system. In *USENIX NSDI*.

Q. Xu, A. Gerber, Z. M. Mao, and J. Pang. 2011. AccuLoc: Practical localization of performance measurements in 3g networks. In *ACM MobiSys*.

L. Yang, Y. Chen, X-Y. Li, C. Xiao, M. Li, and Y. Liu. 2014. Tagoram: Real-time tracking of mobile RFID tags to high precision using COTS devices. In *ACM MOBICOM*.

L. Yang, J. Han, Y. Qi, and Y. Liu. 2010. Identification-free batch authentication for RFID tags. In *IEEE ICNP*.

M. Youssef and A. K. Agrawala. 2005. The Horus WLAN location determination system. In *ACM MobiSys*.

Z. Zhong and T. He. 2009. Achieving range-free localization beyond connectivity. In *ACM SenSys*. 281–294.

G. Zhou, T. He, S. Krishnamurthy, and J. A. Stankovic. 2004. Impact of radio irregularity on wireless sensor networks. In *ACM MobiSys*.

Y. Zhuang, J. Pan, Y. Luo, and L. Cai. 2011. Time and location-critical emergency message dissemination for vehicular ad-hoc networks. *IEEE Journal on Selected Areas in Communications* 29, 1 (2011), 187–196.

Received June 2014; revised October 2014; accepted December 2014